ADVANCED OPTICAL MATERIALS
www.advopticalmat.de

Localized Plasmon Field Effect of Gold Clusters Embedded in Nanoporous Silicon

*Rihan Wu, Thibaut Mathieu, Catherine J. Storey, Qihao Jin, Jack Collins, Leigh T. Canham, and Andrey Kaplan**

Coupling between nanoplasmonics and semiconducting materials can enhance and complement the efficiency of almost all semiconductor technologies. It has been demonstrated that such composites enhance the light coupling to nanowires, increase photocurrent in detectors, enable sub-gap detection, allow DNA detection, and produce large non-linearity. Nevertheless, the tailored fabrication using the conventional methods to produce such composites remains a formidable challenge. This work attempts to resolve that deficiency by deploying the immersion-plating method to spontaneously grown gold clusters inside nano-porous silicon (np-Si). This method allows the fabrication of thin films of np-Si with embedded gold nanoparticles (Au) and creates nanoplasmonic–semiconductor composites, np-Si/Au, with fractional volume between 0.02 and 0.13 of the metallic component. Optical scattering measurements reveal a distinctive, 200 nm broad, localized surface plasmon (LSP) resonance, centered around 700 nm. Linear and non-linear properties, and their time evolution are investigated by optically pumping the LSP resonance and probing the optical response with short wavelength infra-red (2.5 μm) light. The ultrafast time-resolved study demonstrates unambiguously that the non-linear response is not only directly related to the LSP excitation, but strongly enhanced with respect to bare np-Si, while its strength can be tuned by varying the metallic component.

1. Introduction

The combination of nanoplasmonics with semiconductor technology develops a new class of electro-optical materials that not only have attributes of both components, but promises to exhibit new properties, which would be difficult to achieve using each component separately. Plasmonic materials are popular for use in applications and research because they have excellent light absorption cross-section, high electron concentration, and it is possible to tune the resonance wavelength by altering their shape, size, and the environment. Optimized coupling between nanoplasmonics and semiconducting materials can enhance and complement the efficiency of almost all the semiconductor technologies of lasers, solar cells, detectors, sensors, imaging, and electronics. It has been demonstrated that introducing the nanoplasmonics local fields into semiconductor devices enhances the light coupling to nanowires,[1,2] increases photocurrent in germanium detectors,[3] provides means for terahertz all-optical switching,[4] enables sub-gap detection using gold nano-antennas on silicon,[5] allows DNA detection, and[6] produces large non-linearity in epsilon-near-zero material[7] and metasurfaces.[8]

Yet, despite considerable research interest and technological impact, the tailored fabrication of composite material, comprised of a semiconductor with embedded plasmonic nanoparticles, remains a formidable challenge. The conventional mixing techniques used for combining non-conductive dielectrics with metal particles – such as sol-gel, metal-dielectric co-sputtering, metal-ion implantation and pulsed laser deposition, have not been developed to a satisfactory level for semiconductor/metal composites to assure uniformity over metal particles size and density. The lack of the established fabrication techniques hampers the investigation of the plasmon field influence on the charge carrier generation, distribution, decay, and linear and non-linear properties in the semiconductors with embedded clusters supporting the localized surface plasmon (LSP) field.

We attempted to resolve this deficiency and develop a method to fabricate nanoplasmonic-semiconductor composite. We deployed the immersion-plating method to spontaneously grow gold clusters inside nano-porous silicon (np-Si). Although this method is not new, the vast majority of the formerly works employed it to pin metallic particles to the surface. This study is different in that the optical properties and effects of the LSP excitation were investigated for a composite semiconducting material with metallic particles embedded uniformly across its volume. Embedding particles in the volume allows more degrees of freedom to design applications

R. Wu, Dr. T. Mathieu, C. J. Storey, J. Collins,
Prof. L. T. Canham, Dr. A. Kaplan
School of Physics and Astronomy
University of Birmingham
Birmingham B15 2TT, UK
E-mail: a.kaplan.1@bham.ac.uk

Dr. Q. Jin
Light Technology Institute
Karlsruhe Institute of Technology
76131 Karlsruhe, Germany

The ORCID identification number(s) for the author(s) of this article can be found under https://doi.org/10.1002/adom.202002119.

DOI: 10.1002/adom.202002119

and provides more versatile model system to investigate mutual LSP-semiconductor interaction. Importantly, the excitation of nanoplasmonic particles distributed over the volume is more efficient than those pinned to the surface, because a higher amount of clusters can be exposed to a given light flux propagating through a slab. Moreover, a composite made of a material with an enormous surface-to-volume ratio, such as nanoporous silicon[9] and gold clusters embedded inside of it presents benefits to surface enhanced raman spectroscopy. Compared to the more conventional Raman substrates, the number of metal clusters available to enhance the signal will increase by a few orders of magnitude and, in addition to analyte molecules on the surface, there will be an extensive (perhaps even dominant) contribution from those interacting with gold clusters in the pores. Note, that a small fraction of clusters in the pores is unlikely to prevent the diffusion of a solution with analyte over the entire volume of a slab. Nanoporous silicon channels are densely intertwined with a multitude of crossing points where the solution can bypass the clusters blocking locally the passage.

In this work, we investigated the linear and non-linear properties of the np-Si/Au composites optically pumped at the LSP resonance, and probed the optical response and its evolution in time with short wavelength infra-red (SWIR), 2.5 μm, light. This is in contrast to many cases where the electro-optical response of the composites is investigated at or near the LSP resonance. Our work not only focuses on the resonance excitation, but also combines the simultaneous LSP excitation with electro-optical response that was probed in SWIR, away from the resonance. Such approach is useful to decouple the probe beam from the excitation and help to gain insight into the physics of the LSP-semiconductor interaction, dynamics of the resonance, and develop applications.

We show here that the off-resonance extinction of SWIR light propagating through the composite depends linearly on the intensity of light exciting the LSP, as well as on the metal volume fraction. A combination of these two parameters allow freedom to pre-design a thin-film absorber and alter on-demand its optical properties by the LSP excitation–extremely useful quality in the all-optical switching.

We also investigated the SWIR non-linear response of composites and demonstrated that it is strongly enhanced by the LSP excitation. Such unique LSP-induced non-linear properties make the material an excellent candidate for a number of electro-optical applications based on the intrinsic refractive optical bistability. The usefulness of such materials for displays, spatial light modulators, optical image processors, and optical computational elements are known for the decades, in particular in optical elements based on the non-linear Fabry–Perot filters.[10] Our study shows that the composite of porous silicon with the volume fraction of gold of 0.13 in the presence of the LSP excitation nearly fivefold enhances the non-linear refraction with a comparable decrease of the extinction in the SWIR, paving a way to design the active silicon photonics applications with this new class of materials.

Our ultrafast time-resolved study reveals that the recovery of non-linear response is rather limited by a few femtosecond relaxation time of the LSP excitation and the non-linear excitation nearly follows the temporal profile of the pump. The ability to modulate the optical response extremely fast makes the material suitable for all-optical switches/modulators[11,12] and semiconductor saturable absorber mirrors (SESAM's) (the recovery time should be faster than the cavity round trip and non-saturable losses should be small).[13,14] We also show that the non-saturable losses are independent of the metal fraction and tolerable for a wavelength far away from the resonance. In our work, the main losses are attributed to light absorption by the free carriers. The losses are as small as a few percent for a 500-nm-thick sample.

2. np-Si/Au Composite Fabrication and Characterization

2.1. Fabrication and LSP Measurement

In comparison to the previous distinctive works - which also combine the plasmonic material with semiconductors by creating metasurfaces,[7,8] growing noble metal clusters[15] and exploiting nanoantennas on the surface,[3,5] or making a solid solution of metal/semiconductor core/shell structures inside non-conductive transparent matrix[16]—here, we create a hybrid material by incorporating gold nanoclusters inside semiconducting material. np-Si is a natural choice for such an approach. The material fabrication technology demonstrated an excellent record in producing material with precise levels of porosity between 40%and 90%, uniform across areas as large as industrial size wafers. Its optical properties with and without excitation are known[17] and the time-evolution of the excited charge carriers is documented elsewhere.[18,19] In addition, the light scattering by np-Si without gold is insignificant as its roughness parameter, governed by the pores dimensions, is much smaller than the wavelengths comprising the visible and infrared spectra.

Although the use of immersion plating technology to combine gold nanoparticles with np-Si is not original, most of the work reported concerned the decoration of gold nanoparticles onto the surfaces. The deposition of gold nanoparticles inside the pores along the full depth of the channels is less developed or known. In this work, through numerous trials, we overcame difficulties which prevented the precipitation Au-NP into the pores in a controlled manner. The main culprit is an imbalance between the slow diffusion rate of the gold ions solution into the pores and their fast reduction rate, resulting in the deposition on the pore tips.[9] In addition, the process is highly sensitive to concentration, temperature, pore size, internal structure and presence of oxide on the walls.[20–22] By varying the retention time of np-Si substrates in tetrachloroauric acid, optimizing its concentration, removing the native oxide prior to depositions, and promoting the solution diffusion into the pores by ultrasonic bath, we managed to control the Au clusters' density inside the np-Si matrix, while their size to some extent was limited by the pore channel diameter.

Hence, this method has the potential to fabricate materials with a predesigned plasmon resonance wavelength and strength. The degree of porosity controls the effective dielectric function of plasmonic material environment and renormalizes the vacuum resonance wavelength. The form of the pores shapes the gold clusters and influences the resonance strength and width.[23] The np-Si/Au composites that were fabricated in this work have the pore size of 10 to 30 nm, with average cluster size (constrained by the pores dimensions) of 20 nm and

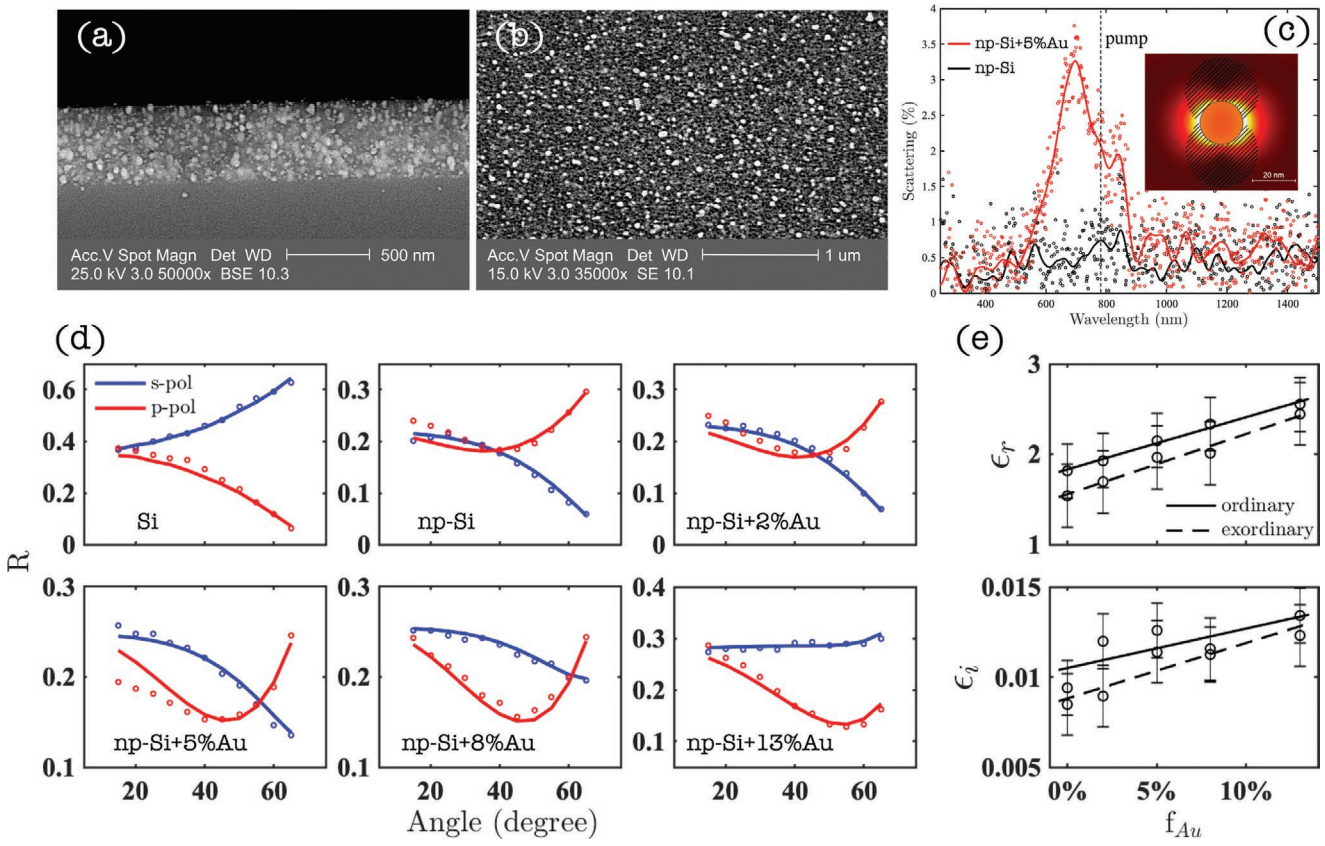

Figure 1. SEM cross-section (a) and top-veiw (b) of np-Si with embedded gold clusters; c) scattering spectrum from np-Si shown by the black dots, and np-Si with embedded gold clusters, $f = 0.05$, shown by the red dots; inset: simulated electric fields distribution around a spherical Au cluster inside np-Si matrix. The line-shaded and colored areas correspond to the probe and pump field intensities distribution, respectively. d) The angular dependence of the reflectance, R, for s- and p-polarized light of 2.5 μm measured on bulk silicon (left top) and np-Si with different fraction of Au clusters, the solid lines are the model fit; e) the effective real and imaginary parts of the dielectric function, ε_r and ε_i, at 2.5 μm.

exhibit ≈200 nm-broad LSP resonance centred around 700 nm, shown in **Figure 1** and Figure S2, Supporting Information.

2.2. Linear Optical Properties in SWIR

The choice to use the 2.5 μm probe was made because of its applications in industry for the inspection of various products as food produce, solar cells, electronic boards, surveillance and anti-counterfeiting, in addition to night-vision devices, imaging scenes illuminated by ambient star light. This wavelength has exquisite qualities for probing the semiconducting environment of metal-nanoclusters composites, namely: 1) the absorption and scattering efficiencies by the metal clusters are strongly suppressed because of extremely small cross-section at this wavelength, governed by the ratio of the particle circumference to the wavelength, $2\pi a/\lambda$[24]; 2) it is below a half of most semiconductors' bandgap; therefore, linear absorption and two photon absorption (TPA) are nearly non-existent; 3) for a strong contrast, $|\varepsilon_c| \gg \varepsilon_e$, between the dielectric functions of the gold clusters, $\varepsilon_c = -288.7 + i14.8$,[25] and np-Si environment, $\varepsilon_e = 1.6$,[17] the probe field is entirely located in the environment surrounding the metal clusters, while penetration into them is diminishing. This point is demonstrated in Figure 1c. Thus, the only interaction of the probe transversing the composite is with the free charge carriers and energetically accessible in-gap states of the np-Si matrix.

We evaluated the optical constants in the SWIR from the reflectance, R_0, measured as a function of the incidence angle for the two principal polarisations, as shown in Figure 1d, for a bare silicon, np-Si substrate, and np-Si with embedded gold clusters. The retrieved real and imaginary parts, ε_r and ε_i, of the effective dielectric function of the np-Si/Au composites and their evolution as the clusters' volume fractions increases from 0 to 13% are displayed in Figure 1e. Each part of the dielectric function is contributed by the ordinary and extraordinary components arising from the weak uniaxial birefringence of the np-Si matrix. It can be seen that at the higher cluster densities, the randomness of their distribution seems to negate slightly the birefringence effect. For the evaluation of the optical constants, we used the Maxwell–Garnett formula, where the effective dielectric function of np-Si was represented as a tensor and gold clusters as isotropic inclusions (see Supporting Information for the calculations details). The fitting used only one free parameter responsible for the clusters' density, while the rest, for the dielectric function of gold, silicon, and porous silicon, were taken from the literature.[25–28] We note the applicability of the Maxwell–Garnett model for np-Si was tested in our previous

works.[17] Figure 1e suggests that despite very large absolute values of the real and imaginary parts of the bulk gold dielectric function, their effect on the optical response of the composite is only fractional, confirming our assertion of the probe field redistribution favourable to interact mainly with the np-Si environment and with little penetration into the clusters.

3. Linear and Non-Linear SWIR Optical Response in the Presence of LSP Resonance Excitation

3.1. Linear Time-Resolved Optical Properties in SWIR

The SWIR probe pulse of ≈200 fs was used to monitor the reflectance change, $\Delta R/R_0$, as a function of time following excitation by the pump pulse near the plasmon resonance at 790 nm (for the experimental details see Experimental Section and Supporting Information). Here, $\Delta R = R(\Delta t) - R_0$ with $R(\Delta t)$ designating the reflectance at time difference Δt between the arrivals of the pump and probe on a sample surface. The zero delay time, $\Delta t = 0$, is assigned to the temporary overlap of the pump and probe arrival time and where the maximum absolute change of the reflectance occurs. The evolution of time resolved spectra during the first 2 ps are shown in **Figure 2**a for bulk silicon and np-Si with different loads of the clusters for comparison. It can be seen that all samples after the zero delay, with the exception of the bulk silicon, show a negative change. In semiconductors, this indicates that the carrier (electron and hole) density increased, but the corresponding plasma frequency is below that of the probe light. The complete recovery of the signal is not shown because the excited carrier decay time is about 100 ps,[18] much longer than the time scales investigated here. Therefore, we can also eliminate the recombination process and possible alteration of its mechanism from the factors affecting the observed initial signal recovery around the zero delay. The investigated time scales are by orders of magnitude too short to accommodate sub-nanoseconds decay time of the excited charge carriers in semiconductors even when this can be further shortened or artificially enhanced by the LSP or by presence of the gold particles as additional recombination sites in the matrix.

Comparing the response of the samples with and without gold clusters, excited by 790 nm wavelength located within the range of the plasmon resonance band (Figure 2a), one notes two striking differences: at a given pump intensity, the reflectance change and the initial recovery time are enhanced for the material containing gold clusters. These effects increase when the density of the gold clusters increases. As opposed to the excitation by a wavelength of 1.1 µm, which is outside of the LSP resonance band, and using the same probe, where the dynamics of the optical response is identical for the samples with and without embedded gold nanoparticles, see Figure S3, Supporting Information.

For a meaningful discussion of these results, we deduced the effective real, ε_r, and imaginary, ε_i, parts of the dielectric function at the maxima of the reflectance absolute change and plotted them in Figure 2b as a function of the pump fluence. The obtained dependence can be explained within the framework of the Drude model for the specific conditions of the probe frequency being greater than the electron–hole plasma frequency and the free carrier scattering rate, $\omega > \omega_p$, $1/\tau$. At these conditions, the model approximates the real and imaginary parts of the dielectric function dependencies as $\varepsilon_r - \frac{\omega_p^2}{\omega^2}$ and $\varepsilon_i + \frac{\omega_p^2}{\omega^3\tau}$, respectively.[29] The plasma frequency is given by $\omega_p^2 = \frac{e^2}{\varepsilon_0}\frac{N}{m_{\text{eff}}}$, where the carrier density, N, is determined by the pump intensity, I_{pump}, and absorption coefficient of composite, α_{pump}, as $N \propto \alpha_{\text{pump}} I_{\text{pump}}$; m_{eff} is the effective mass of the electron–hole plasma in silicon.

We note that despite the presence of gold clusters, the contribution of their dielectric function and its change due to the excitation by the pump does not significantly affect the optical response of the composite and does not have to be considered here. Indeed, the probe optical response is governed exclusively by the np-Si environment. This is because for the condition of $|\varepsilon_c| \gg \varepsilon_e$, the Maxwell–Garnett mixing can be approximated to represent the effective dielectric as $\varepsilon_{\text{eff}} = \varepsilon_r + i\varepsilon_i \approx \varepsilon_e(1 + 2f)$, where f is a volume fraction of the gold clusters. Moreover, the

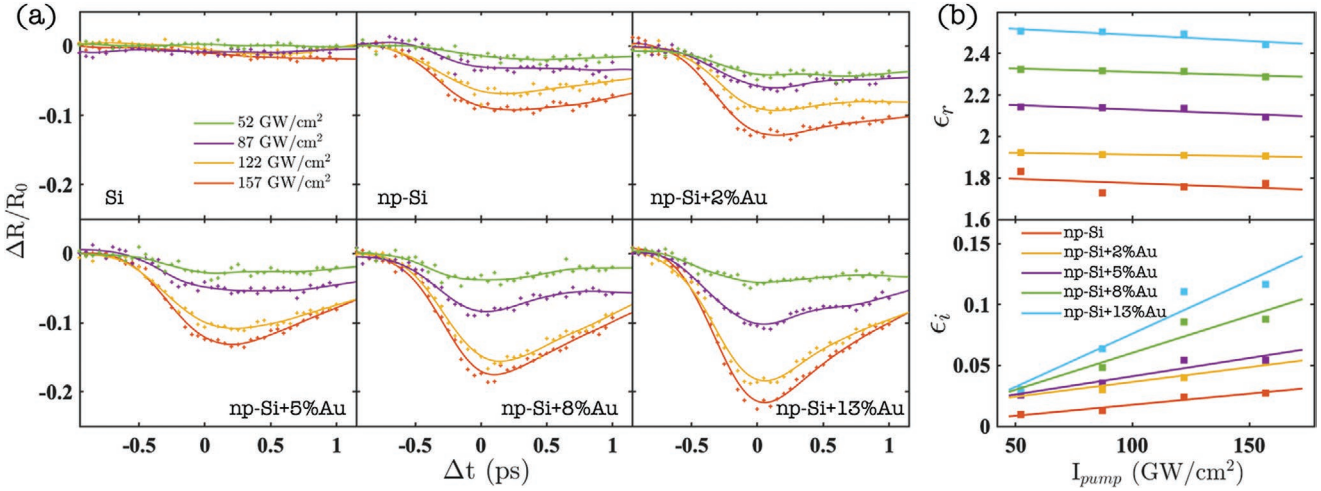

Figure 2. a) Time-resolved reflectance change, $\Delta R/R_0$, for the different intensities of the 790-nm-pump and 2.5 µm fixed-intensity probe; b) the dependence of the real and imaginary parts, ε_r and ε_i, of the effective dielectric function on the pump intensity, I, for np-Si with different density of Au clusters.

excitation of the gold clusters by the pump does not considerably change their dielectric function, even at the conditions of the LSP resonance. At sub-picoseconds timescales, the change of the dielectric function is governed by the electron density, N_{noneq}, driven out of the equilibrium by the pump. This density can be estimated by $N_{\text{noneq}} = \tau_{\text{LSP}}\alpha_{\text{Au}}\frac{I_{\text{pump}}}{\hbar\omega_{\text{pump}}}$. Using the LSP dephasing time, τ_{LSP} of 5 fs,[30] a gold cluster absorption coefficient of $\alpha_{\text{Au}} = 1.5 \times 10^6$ cm^{-1},[31,32] it can be found that a fraction of 0.03 of the total charge density participate in the LSP excitation at the pump frequency. This fraction is too minor to alter the dielectric function of the gold clusters.

It can be estimated that the cluster and matrix heating are the secondary effects dominated by the relaxation of the excited carriers and LSP. Indeed, assuming that the small fraction of the free carriers absorbs the maximum allowed photon energy of 1.5 eV each, we can calculate that 20 nm diameter cluster initially absorbs $\Delta E \approx 11 \times 10^3$ eV of the pump energy. This is followed by redistribution of this energy among the entire charge carriers system establishing the electronic temperature of about 580 K above the ambient conditions. Such extra energy is not sufficient to overcome the barrier of 0.4 eV between silicon and gold. Therefore, no charge transfer is possible via thermal excitation of gold. In addition, one can estimate the lattice temperature of gold and the change of the related refractive index. Assuming, that the charge carriers are able to transfer the excess energy to the lattice without losses, we can find that the temperature rises by $\Delta T = \frac{\Delta E}{mc} = 175$ °C, where $m = 8 \times 10^{-17}$ g and $c = 0.127$ J g^{-1} °C^{-1} are the mass of a particle and gold heat capacity, respectively. However, this is the highest possible temperature which particle can achieve when no energy outflows into the surrounding. In reality, the energy escapes from particles into the silicon surrounding, thus the final temperature is even lower at least a half. Such change of the temperature in semiconducting matrix and gold particles is difficult to observe as the thermo-optical coefficients are about 10^{-4}. Possible changes to the refractive indices by their heating is just a few pro mille and are masked by much stronger contributions of the electronic density and scattering time in Drude response.

Therefore, a simplified expression for ε_{eff}, which does not need to involve ε_c, can be used to investigate the dependence of ε_r and ε_i on the pump intensity, I_{pump}, for a given f. It can be seen on Figure 2b that the slopes of the curves family, $\varepsilon_i(I_{\text{pump}}; f)$, given by $\frac{e^2}{\varepsilon_0}\frac{N}{m_{\text{eff}}}\frac{1}{\omega^3\tau}$, tend to increase as the volume fraction of gold clusters, f, grows. It is rather tempting to attribute this to the enhancement of the carrier excitation by the pump and increase of N in the samples with greater amount of the clusters. However, there are two arguments against this notion. First, it is not corroborated by the slopes of the $\varepsilon_r(I_{\text{pump}}; f)$ set given by $-\frac{e^2}{\varepsilon_0}\frac{N}{m_{\text{eff}}}\frac{1}{\omega^2}$, which have insignificant dependence on the parameter f. Second, the time-resolved curves shown in Figure 2a demonstrate the identical tendency to recover to nearly the same value of $\Delta R/R_0$ after 1 ps from the extremum, irregardless of the embedded clusters' density. This point is confirmed by another independent set of measurements shown in **Figure 3**a. Hence, on the average across the sample, the presence of the LSP field around the clusters neither enhances the excitation efficacy of the free carriers average density nor promotes charge transfer from gold to the surrounding silicon to affect the decay rate of the electron-hole pair in np-Si environment.

Thus, the change of the linear optical properties of np-Si in the presence of gold cluster's LSP excitation is mainly governed by the alteration of the imaginary part of the composite effective dielectric function, ε_i, where, as our analysis suggests, the dominant effect is nested in the change of the electron-hole plasma relaxation rate, $1/\tau$. It seems that this rate tends to increase as the gold fraction, f, increases and, hence, the contribution of the LSP to this effect, for a given pump power, I_{pump}.

We verified this effect presenting the relaxation rate, $1/\tau$, as a function of the cluster's fraction, f, shown in Figure S4 in the Supplementary Materials. It suggests a linear dependence for which the LSP more than threefold enhances the charge carriers' scattering rate for the cluster's fraction of $f = 0.13$. The investigation of the reasons behind the enhancement is beyond the scope of this work, however we note that the LSP oscillating field might have broadened the free carriers energy distribution and increased their carrier-carrier collision rate.

There is another revealing point which can be demonstrated from $\Delta R/R_0$ time resolved curves. Deconvoluting the response of the pure np-Si from the curves measured on the composites separates the temporal contribution of the LSP and unveils a symmetric bell-shaped curve, similar to the shape of a slightly broadened pump pulse, shown in Figure S5, Supporting Information. Hence, the fast recovery of $\Delta R/R_0$ following the extremum is rather governed by the LSP relaxation, while the long tail extending into hundreds of picoseconds is attributed to the decay of the electron-hole plasma in np-Si matrix. It is very likely the LSP is as short lived as a few femtoseconds and it nearly adiabatically follows the excitation pulse.

3.2. Non-Linear Response in SWIR

Furthermore, the dependence of τ on the external perturbation strongly suggests that the optical response can be significantly non-linear, as, for example, it was shown in the epsilon-near-zero materials.[33,34] We investigated non-linear response to the SWIR probe in the presence of the LSP excitation by the pump. For this series of experiments, the pump intensity was kept at the constant level of 160 GW cm^{-2}, but the probe was tuned in the range between 3.5 and 27 GW cm^{-2} (see Figure 3a). Here, we see that increasing the probe intensity has the opposite effect to that of the pump shown in Figure 2a. That is, the absolute reflectance change, $|\Delta R/R_0|$, instead decreases as a function of the intensity. However, at longer time delays, past the localized surface plasmon decay time, there is no difference in the response between the samples with and without the clusters. Indeed, regardless of the composition, after 2 ps all time-resolved curves appear as a nearly identical long tail. On the contrary, the fast component has a substantial dependence of the $|\Delta R/R_0|$ on the gold fraction, f, for a given probe intensity around the zero delay time.

This observation confirms our proposal that the distinctive change to the optical response can be observed only during short time period of the LSP excitation. The measurements clearly demonstrate that the probe intensity-dependent

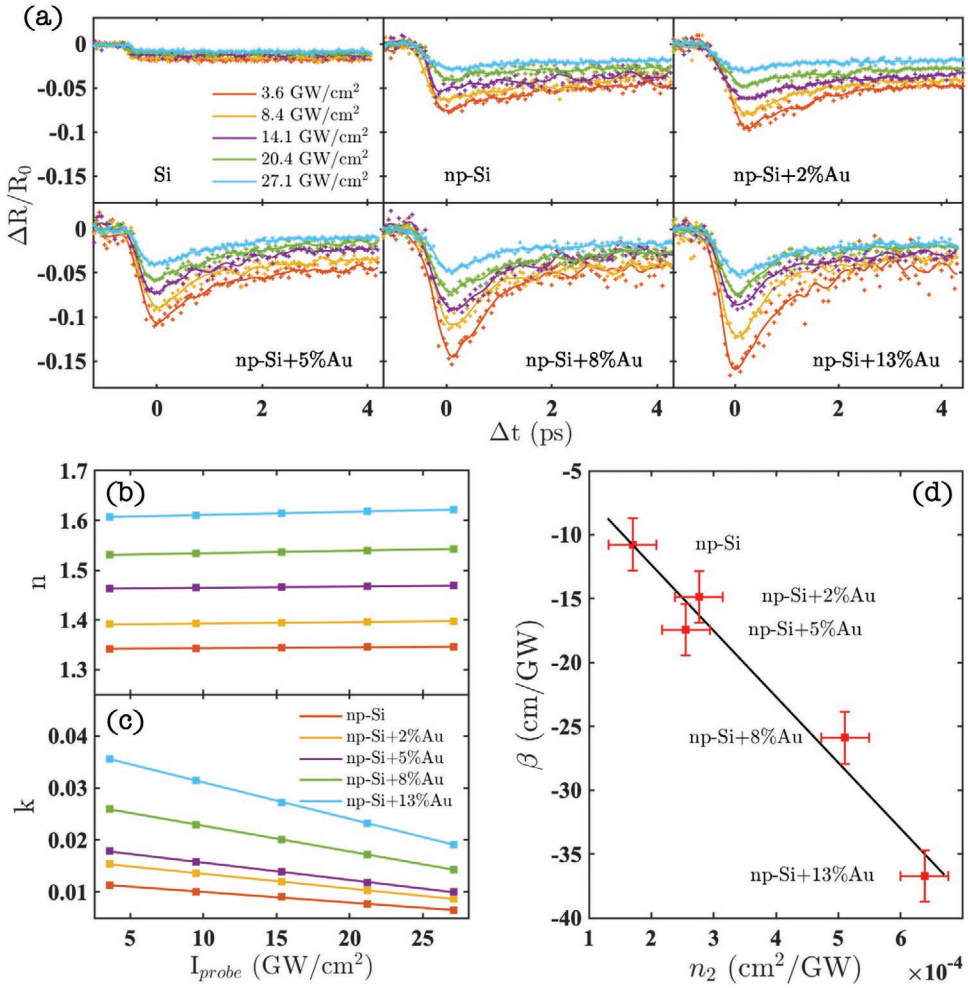

Figure 3. a) Time-resolved reflectance change, $\Delta R/R_0$, for the fixed pump intensity of 160 GW/cm^2 and different intensities of the probe; b) the real and c) the imaginary parts, n and k, of the effective refractive index as a function of the 2.5 μm probe intensity; d) non-linear Kerr and extinction indices, n_2 and β, for np-Si with different densities of Au clusters.

response is at a maximum at the time corresponding to the temporal overlap between the pump and probe pulses. It is also very clear that the strongest change occurs in the samples with the highest density of the clusters where more free charges in the matrix are exposed to the LSP field.

We evaluated the effective refractive index at the maxima of the time-resolved reflectance change and present its real, n, and imaginary, k, parts as a function of the probe intensity, I_{probe}, in Figure 3b,c. The slopes are determined by the non-linear indices of n_2 and β,[35] the real and imaginary parts of the non-linear refraction, which are shown in Figure 3d. The investigated samples show that n_2 is positive, corresponding to Kerr non-linear self-focusing, while a negative β is usually associated with the absorption saturation or bleaching. Here, we note that the observed non-linearity is exclusively attributed to the free carriers excited by the pump, as without pumping neither material demonstrates significant non-linearity at the investigated probe intensities.

There is no established way to predict the free carriers response in the presence of LSP fields. As well, it is a very complex task to discern the underpinning mechanism of the free carriers' non-linear response in semiconductors, as it may originate from the twisted together factors determining the values of the reduced mass, screening and relaxation. The exercise is further hindered when the process occurs in non-equilibrium state with poorly defined distribution of the carriers. It is known from decades of bulk silicon research that free carrier absorption in a p-type degenerated material consists of two competing components of the more familiar intraband and featured intervalence split-off band free carrier transitions[36] (see the diagram in Figure S6, Supporting Information. The former transition is known to saturate at a relatively high pumping level of two-to-three orders of magnitude above our work[37] and it might not be suitable to explain our observation. On the other hand, the intervalence transition is more sensitive as it depends on the product of occupation probabilities in two non-degenerate bands involved in the transition and it is known to saturate rapidly at above 5× 10^{18} cm^{-3}. np-Si with weak carrier confinement preserves many of the bulk silicon electro-optical properties and the absorption saturation can be recognised from the decrease of the reflectance change as a function of the increasing probe intensity in Figure 3a. This effect is further enhanced with embedding gold clusters into the np-Si matrix, but it is only temporarily efficient during the time

window of the localized plasmon excitation. It is very likely that the effect of the absorption saturation enhancement is the result of disturbing the free carriers distribution and population probability in a way that fewer states are available for the intervalence split-off band transitions of the free charge carriers.

Overall, the efficiency on the non-linear enhancement should be judged against the response of the bare porous silicon at the identical conditions. Incorporation of just 0.13 of gold volume fraction not only more than fivefold enhances the non-linear optical response in the presence of the LSP excitation, but also shorten the recovery time by an order of magnitude, allowing implementation of the effect in applications where the high-speed response is essential.

4. Conclusion

We demonstrated that adoption of the immersion plating technique allows—in a reasonably controlled manner—the incorporation of gold clusters into a nanoporous silicon with pore diameter of a few tens of nanometers. We investigated optical linear and non-linear responses at 2.5 μm of the SWIR range while exciting simultaneously the localized surface plasmon, supported by the gold clusters and free carriers across the band gap, using 790 nm pump. We proposed that the local fields of the LSP are likely to disturb the excited free carriers energy distribution in the semiconducting matrix and enhance the relaxation rate and saturation of the SWIR probe absorption. The effect is enhanced as the gold cluster density in the matrix increases. This process is very fast and it is only observable in the presence of the local plasmon excitation, which tends to decay immediately with the rolling-off of the pump pulse. Therefore, for the applications, one can model a temporal profile of a non-linear response that follows the shape of the pump exciting the LSP.

5. Experimental Section

Porous Silicon Fabrication: Nano-porous silicon samples were prepared using electrochemical anodization of a boron doped Si (100) wafer with resistivity in the range of ≈5–20 mΩ cm, corresponding to a dopant density of $\approx 3 \times 10^{18}$ cm^{-3}. A 1:1 ratio mixture of methanol and 40% hydrofluoric acid was used as the electrolyte at a current density of 100 mA cm^{-2} for 8 s to yield a np-Si layer with thickness of approximately 550 nm (measured from the cross-section of SEM image). Each sample was rinsed thoroughly with methanol and dried in air after the electrochemical etch. A 65% porosity was estimated using a gravimetric method.[26]

Impregnation of Gold Cluster into Porous Silicon Matrix: An electroless immersion plating technique was used to impregnate gold clusters into the np-Si layer, using an immersion solution prepared by dissolving 9.85 mg of tetrachloroauric(III) acid ($HAuCl_4$) in 50 mL of ethanol, producing a concentration of 0.5 mM. Before the impregnation process, the np-Si samples were dipped in 2% of HF (diluted in DI water) for 30 s to remove the native oxide layer developed on the surface of the sample and inside the pores. Afterward, the np-Si samples were immersed in the pre-mixed $HAuCl_4$ solution and placed in an ultrasonic bath to agitate the solution and stimulate it to penetrate into the pores. After a chosen time period, the samples were rinsed in ethanol and dried in air. There are a few parameters which can control the metallic environment furnishing this system with extra flexibility. The pore size controls the largest possible particle diameter, while the porosity similarly governs the highest density. On the other hand, particles smaller and less dense than the pores can be made by shortening the retention of the samples in the solution. To achieve uniform distribution, the temperature was maintained during deposition at 25 °C, where the diffusion rate of solution in porous silicon and reduction rate were balanced for $HAuCl_4$ concentration not greater than 1 mM. **Table 1** shows the acid concentration and immersion times for the samples used in the experiments. Scanning electron microscopy was used to observe the presence of gold clusters in the samples cross-section. Figure S2, Supporting Information, shows a representative example of the SEM cross section image of the np-Si+2%Au sample, where Au clusters can be seen inside the np-Si pore channels. The random points analysis of the SEM images suggest that the mean diameter of the clusters in this sample is about 20 nm. In addition, the analysis suggests that the np-Si pore channel diameter and the wall (silicon skeleton) thickness are both in the range of 10–30 nm, indicating a weak quantum confinement with diminishing effect on the np-Si electronic structure.

Table 1. List of $HAuCl_4$ concentrations and immersion times used for the preparation of nano-composite samples. The Au concentration was determined from reflectometry measurements (Figure 1) and Section SIIIB, Supporting Information.

Sample	$HAuCl_4$ concentration	Immersion time	Au volume fraction [*f*]
np-Si/Au 1	0.5 mM	10 min	0.02
np-Si/Au 2	1 mM	20 min	0.05
np-Si/Au 3	1 mM	120 min	0.08
np-Si/Au 4	1 mM	720 min	0.13

Localized Surface Plasmon Spectroscopic Measurements: A broad band unpolarized white light source was used to illuminate the samples, while back-scattered light was collected by a PerkinElmer Lambda 1050 UV/vis/NIR spectrometer equipped with an integrating sphere. The samples were placed at the back of the sphere where the light was reflected back off the sample and collected by the sphere. To exclude the specular component from the diffuse scattered reflectance, a corresponding aperture was opened on the port which allowed the specularly reflected light to exit the sphere.

The LSP resonance position is peaked at 700 nm, shown in Figure 1c. The resonance is red-shifted in comparison to the more familiar location between 500 and 600 nm for gold particles suspended in a vacuum or a medium with low dielectric constant.[38] Here, the particles surrounded by a shell of silicon with the real part of dielectric function of $\varepsilon^r_{Si}(\lambda = 700\ nm) = 14.3$,[39] shifting the resonance to a longer wavelength. The position of the resonance can be estimated according to the conditions $\varepsilon^r_{Si} + \varepsilon^r_{Au} \approx \varepsilon^i_{Au}$. The dielectric function for gold nanoparticles is not known exactly, but for the sake of the approximation, the value known for a few nm-thick gold film, $\varepsilon_{Au}(\lambda = 700\ nm) \approx -10 + i4$[40] can be used, for which the conditions of the resonance can be fulfilled. It is noted that this estimate should be regarded as a rough approximation, which assumes particles as ellipsoids excited along the minor axis and disregarding contribution from the major axis. As well, it supposes that the LSP field is entirely located in the silicon environment, disregarding further penetration into neighbouring hollow pores or interaction with other gold particles. More detailed calculations exploring the position and shape of the resonance spectra is a subject of further investigation.

Simulation of the Pump and Probe Electric Fields Distributions: Comsol Mulitiphysics was used for the simulation of the localized field distribution in the vicinity of an Au particle. The particle size was set to 20 nm, surrounded by silicon, emulating the pore walls. The pump and probe wavelengths were the same as in the experiment, 790 and 2.5 μm, respectively. The pump and probe were orthogonally polarized. The simulation suggested that the pump field is uniform inside the particle and decays into the surrounding silicon over the factor of $1/e$ within 5 nm. The pump field is an order of magnitude amplified on the edge of the particle with respect to the imposed field. On the other hand, the probe field inside the particle is nearly zero but extends to a longer decay distance of 20 nm. Its field is also enhanced, albeit by rather small factor of 2.5. It was noted that, in this work, the interaction between LSP fields of neighboring clusters can be ignored because, for the Au highest volume fraction of 0.13, the average distance between particles is more than 30 nm, at which the field, imposed by the pump, decays to an asymptote.

NIR-Pump – SWIR-Probe Measurements: The continuous, time-resolved, and non-linear measurements in SWIR were performed using a Coherent ultrafast laser system. Intensive fundamental laser pulses—with 790 nm central wavelength, 60 fs duration, and average power of 3 W—were produced by a regenerative amplifier. Using a beam splitter, the smaller fraction of the beam (about 5%) was used as the pump beam to excite the LSP on gold clusters and free charge carriers in the np-Si matrix simultaneously. The remnant of the beam was guided into an optical parametric amplifier (OPerA-Solo) to generate a probe beam with the wavelength of 2.5 μm and pulse duration of about 200 fs.[18,41] The optical path length of the pump beam was precisely adjusted by a computer-controlled retroreflector, in order to adjust and scan the temporal overlap between pump and probe on the sample. The pump beam spot diameter on the sample was about 1 mm and the probe spot diameter was set to 600 μm. Both the pump and probe intensity were controlled by rotating half-wave plates in front of linear polarizers which also set the beam polarization. The pump beam was set to p-polarized, while the probe beam was adjusted to be orthogonally polarized with respect to the pump to prevent interference between them. The incident angles of the pump and probe beams were set to 30° and 20°, respectively. The transient reflection of the probe beam was detected by a PbS detector (detector 1), while another balanced detector (detector 2) was used to monitor the fluctuations of the beam intensity. Both of these detectors were connected to a Zurich Instrument lock-in amplifier and the recorded data was read out by a LabVIEW program. The schematics of the setup are shown in Figure S1, Supporting Information.

Supporting Information

Supporting Information is available from the Wiley Online Library or from the author.

Acknowledgements

The authors thank Dstl for financial support enabled by the grant DSTLX100099482.

Conflict of Interest

The authors declare no conflict of interest.

Data Availability Statement

The data that support the findings of this study are available from the corresponding author upon reasonable request.

Keywords

localized surface plasmon, non-linear optics, porous silicon, semiconductor–metal composite

Received: January 5, 2021
Revised: February 3, 2021
Published online: February 24, 2021

[1] S. Mokkapati, D. Saxena, N. Jiang, P. Parkinson, J. Wong-Leung, Q. Gao, H. H. Tan, C. Jagadish, *Nano Lett.* **2012**, *12*, 6428.
[2] A. Casadei, E. F. Pecora, J. Trevino, C. Forestiere, D. Rüffer, E. Russo-Averchi, F. Matteini, G. Tutuncuoglu, M. Heiss, A. Fontcuberta i Morral, L. Dal Negro, *Nano Lett.* **2014**, *14*, 2271.
[3] L. Tang, S. E. Kocabas, S. Latif, A. K. Okyay, D.-S. Ly-Gagnon, K. C. Saraswat, D. A. B. Miller, *Nat. Photonics* **2008**, *2*, 226.
[4] M. Ren, B. Jia, J.-Y. Ou, E. Plum, J. Zhang, K. F. MacDonald, A. E. Nikolaenko, J. Xu, M. Gu, N. I. Zheludev, *Adv. Mater.* **2011**, *23*, 5540.
[5] M. W. Knight, H. Sobhani, P. Nordlander, N. J. Halas, *Science* **2011**, *332*, 702.
[6] S.-W. Ryu, C.-H. Kim, J.-W. Han, C.-J. Kim, C. Jung, H. G. Park, Y.-K. Choi, *Biosens. Bioelectron.* **2010**, *25*, 2182.
[7] M. Z. Alam, S. A. Schulz, J. Upham, I. De Leon, R. W. Boyd, *Nat. Photonics* **2018**, *12*, 79.
[8] M. Ren, W. Cai, J. Xu, *Adv. Mater.* **2020**, *32*, 1806317.
[9] L. Canham, *Handbook of Porous Silicon*, Springer, New York **2014**.
[10] B. S. Wherrett, S. D. Smith, *Phys. Scr.* **1986**, *T13*, 189.
[11] C. Koos, P. Vorreau, T. Vallaitis, P. Dumon, W. Bogaerts, R. Baets, B. Esembeson, I. Biaggio, T. Michinobu, F. Diederich, W. Freude, J. Leuthold, *Nat. Photonics* **2009**, *3*, 216.
[12] R. Wu, J. Collins, C. D, Burgess, R. A. Lamb, A. Kaplan, *Proc. SPIE* **2018**, *10799*, 1079904.
[13] U. Keller, K. J. Weingarten, F. X. Kartner, D. Kopf, B. Braun, I. D. Jung, R. Fluck, C. Honninger, N. Matuschek, J. Ausder Au, *IEEE J. Sel. Top. Quantum Electron.* **1996**, *2*, 435.
[14] H. A. Haus, *J. Appl. Phys.* **1975**, *46*, 3049.
[15] S. Tan, A. Argondizzo, J. Ren, L. Liu, J. Zhao, H. Petek, *Nat. Photonics* **2017**, *11*, 806.
[16] S. K. Cushing, J. Li, F. Meng, T. R. Senty, S. Suri, M. Zhi, M. Li, A. D. Bristow, N. Wu, *J. Am. Chem. Soc.* **2012**, *134*, 15033.
[17] W. He, I. V. Yurkevich, L. T. Canham, A. Loni, A. Kaplan, *Opt. Express* **2014**, *22*, 27123.
[18] A. Zakar, R. Wu, D. Chekulaev, V. Zerova, W. He, L. Canham, A. Kaplan, *Phys. Rev. B* **2018**, *97*, 155203.
[19] W. He, A. Zakar, T. Roger, I. V. Yurkevich, A. Kaplan, *Opt. Lett.* **2015**, *40*, 3889.
[20] F. Ronkel, J. W. Schultze, R. Arens-Fischer, *Thin Solid Films* **1996**, *276*, 40.
[21] F. Zacharatos, A. G. Nassiopoulou, *Phys. Status Solidi A* **2008**, *205*, 2513.
[22] M. Zhao, F. Shadman, M. Keswani, *Appl. Surf. Sci.* **2018**, *445*, 505.
[23] K. L. Kelly, E. Coronado, L. L. Zhao, G. C. Schatz, *J. Phys. Chem. B* **2003**, *107*, 668.
[24] H. C. Hulst, H. C. van de Hulst, *Light Scattering by Small Particles*, Courier Corporation, New York **1981**.
[25] S. Babar, J. H. Weaver, *Appl. Opt.* **2015**, *54*, 477.
[26] R. Wu, J. Collins, L. T. Canham, A. Kaplan, *Appl. Sci.* **2018**, *8*, 1810.
[27] V. Y. Timoshenko, L. Osminkina, A. Efimova, L. Golovan, P. Kashkarov, D. Kovalev, N. Künzner, E. Gross, J. Diener, F. Koch, *Phys. Rev. B* **2003**, *67*, 113405.
[28] A. D. Rakić, A. B. Djurišić, J. M. Elazar, M. L. Majewski, *Appl. Opt.* **1998**, *37*, 5271.
[29] J. M. Ziman, *Principles of the Theory of Solids*, Cambridge University Press, Cambridge, UK **1972**.
[30] A. O. Govorov, H. Zhang, H. V. Demir, Y. K. Gun'ko, *Nano Today* **2014**, *9*, 85.
[31] G. Rosenblatt, B. Simkhovich, G. Bartal, M. Orenstein, *Phys. Rev. X* **2020**, *10*, 011071.
[32] C. F. Bohren, *Am. J. Phys.* **1983**, *51*, 323.
[33] A. D. Neira, N. Olivier, M. E. Nasir, W. Dickson, G. A. Wurtz, A. V. Zayats, *Nat. Commun.* **2015**, *6*, 7757.
[34] M. Z. Alam, I. De Leon, R. W. Boyd, *Science* **2016**, *352*, 795.
[35] R. W. Boyd, *Nonlinear Optics*, Elsevier, New York **2008**.
[36] L. M. Lambert, *Phys. Status Solidi A* **1972**, *11*, 461.
[37] K. Sokolowski-Tinten, D. von der Linde, *Phys. Rev. B* **2000**, *61*, 2643.
[38] P. B. Johnson, R. W. Christy, *Phys. Rev. B* **1972**, *6*, 4370.
[39] D. E. Aspnes, A. A. Studna, *Phys. Rev. B* **1983**, *27*, 985.
[40] D. I. Yakubovsky, Y. V. Stebunov, R. V. Kirtaev, G. A. Ermolaev, M. S. Mironov, S. M. Novikov, A. V. Arsenin, V. S. Volkov, *Adv. Mater. Interfaces* **2019**, *6*, 1900196.
[41] R. Wu, J. Collins, D. Chekulaev, A. Kaplan, *Appl. Sci.* **2019**, *9*, 1808.